Electronic Supplementary Information (ESI)

Probing the limits of linker substitution in aluminum MOFs through water vapor sorption studies: Mixed-MOF instead of mixed-linker CAU-23 and MIL-160 materials

Carsten Schlüsener, Dustin Nils Jordan, Mergime Xhinovci, Tobie J. Matemb Ma Ntep, Alexa Schmitz, Beatriz Giesen, Christoph Janiak*

Institut für Anorganische Chemie und Strukturchemie, Heinrich-Heine-Universität, D-40204 Düsseldorf, Germany.

Keywords

metal-organic framework (MOFs), mixed-linker, thiophenedicarboxylic acid, furandicarboxylic acid, water sorption

E-Mails: carsten.schluesener@hhu.de; dustin.jordan@hhu.de; mergime.xhinovci@hhu.de; tobie.matemb.ma.ntep@hhu.de; alexa.schmitz@hhu.de; beatriz.giesen@hhu.de; janiak@hhu.de

Table of Contents

S1. Brief description of cycling heat transformation with thermally driven adsorption heat pumps (AHPs)

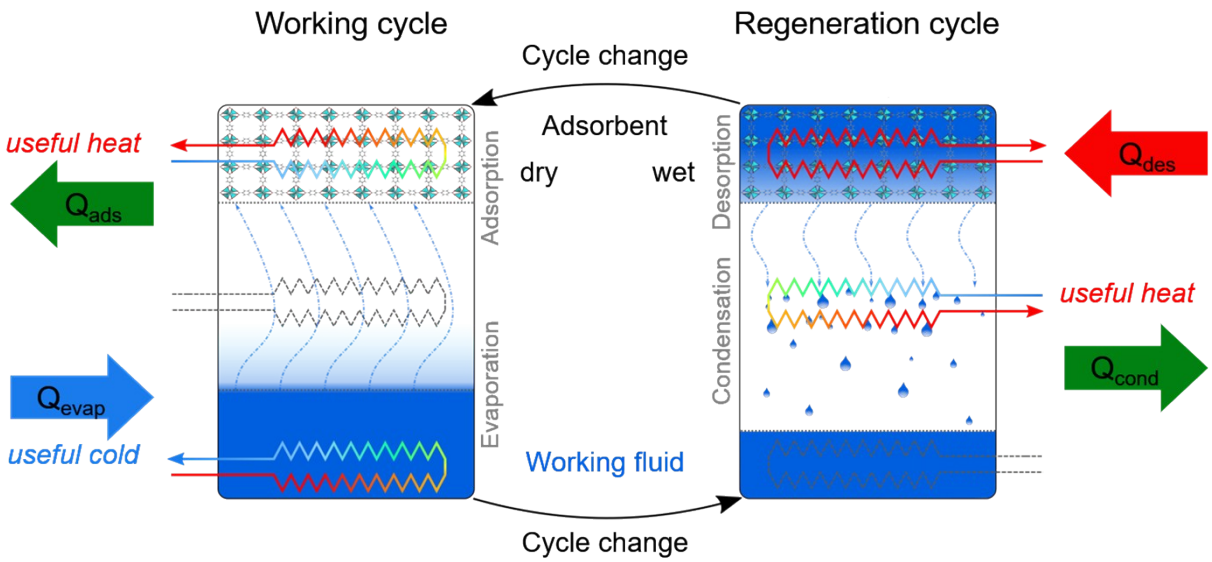

Scheme S1 Working scheme of a sorption-based chiller/heat pump. In the working cycle, a working fluid (favorably water due to its high evaporation enthalpy and nontoxicity) is evaporated, taking up heat of evaporation Q_{evap} which translates into useful cold. During adsorption into a porous material, heat of adsorption Q_{ads} is released. In the regeneration cycle, driving heat Q_{des} for desorption is applied, and condensation takes place at a medium temperature level and releases condensation heat Q_{cond}. The device can be used as a chiller or a heat pump.

S2. Brief description of relevant metal-organic frameworks in this work

MIL-160

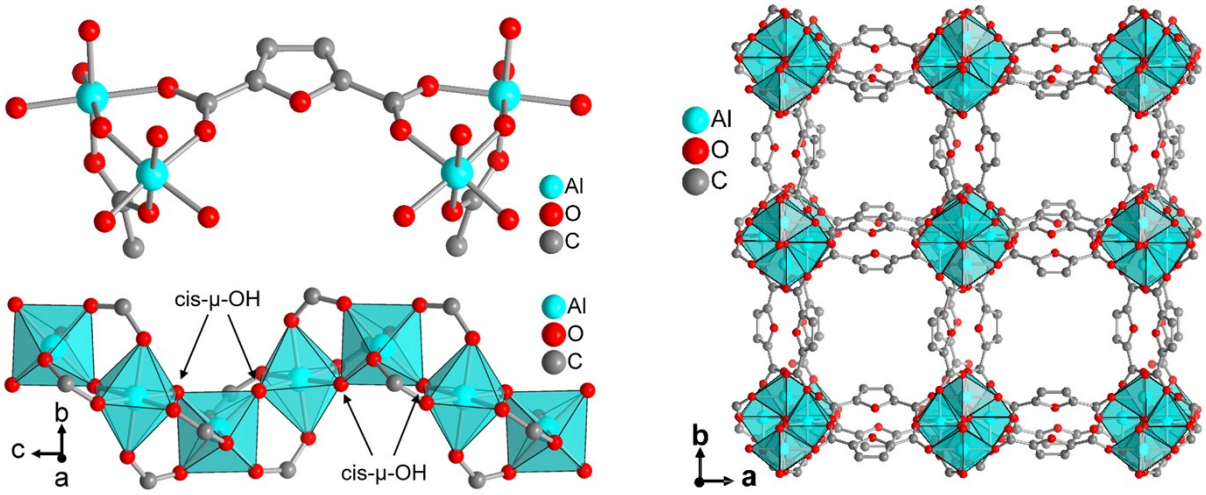

Fig. S1 Structural elements in MIL-160 (isostructural to CAU-10-H) with extended asymmetric unit, the fourfold helical chain of cis vertex-bridged {AlO_6}-polyhedra as the inorganic building unit, and the 3D framework structure of square-shaped one-dimensional channels. Graphics produced from cif-file for MIL-160 (CSD-Refcode PIBZOS).[1]

CAU-10-H

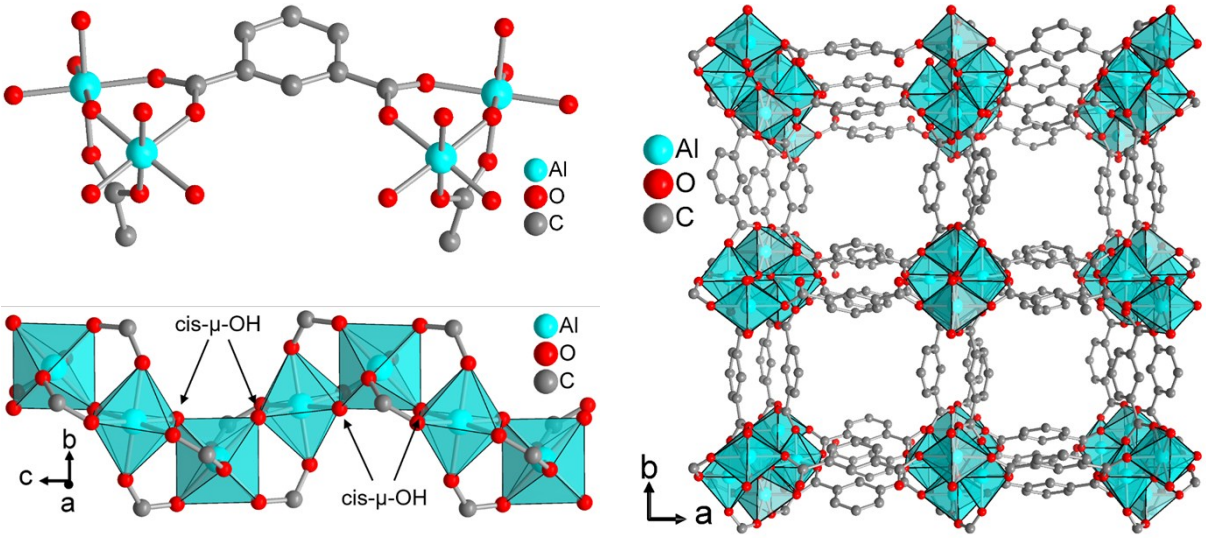

Fig. S2 Structural elements in CAU-10H(dry) (isostructural to MIL-160) with extended asymmetric unit, the fourfold helical chain of cis vertex-bridged {AlO_6}-polyhedra as the inorganic building unit, and the 3D framework structure of square-shaped one-dimensional channels. Graphics produced from cif-file for CAU-10-H(dry) (CCDC 1454067, CSD-Refcode OQOCAA)[2]

CAU-23

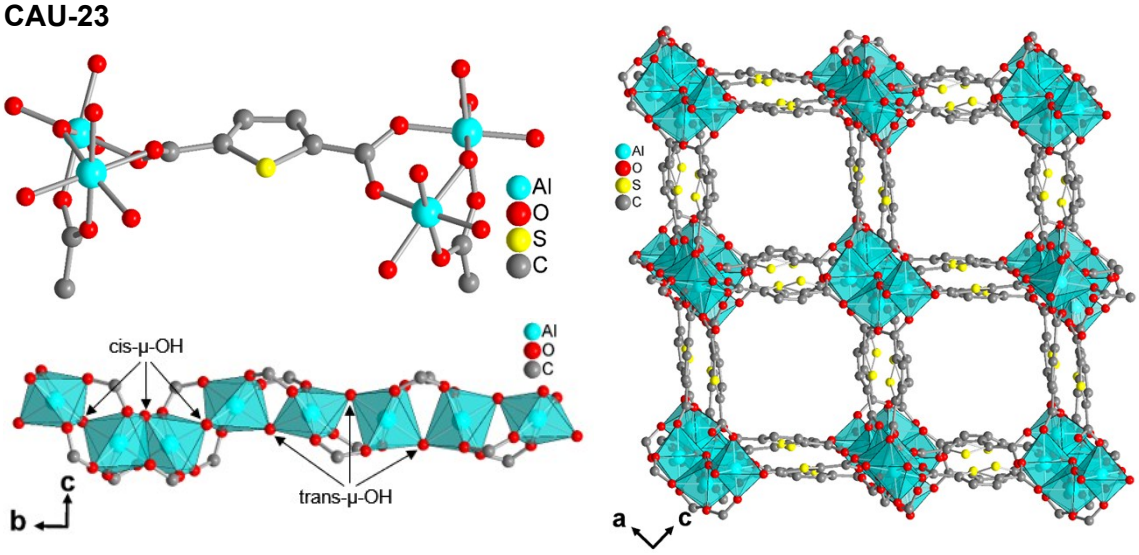

Fig. S3 Structural elements in CAU-23 with extended asymmetric unit, the fourfold helical chain of cis and trans-vertex-bridged {AlO_6}-polyhedra as the inorganic building unit, and the 3D framework structure of square-shaped one-dimensional channels. Graphics produced from cif-file for CAU-23 (CSD-Refcode ZOVHUQ).[3]

MIL-53-TDC

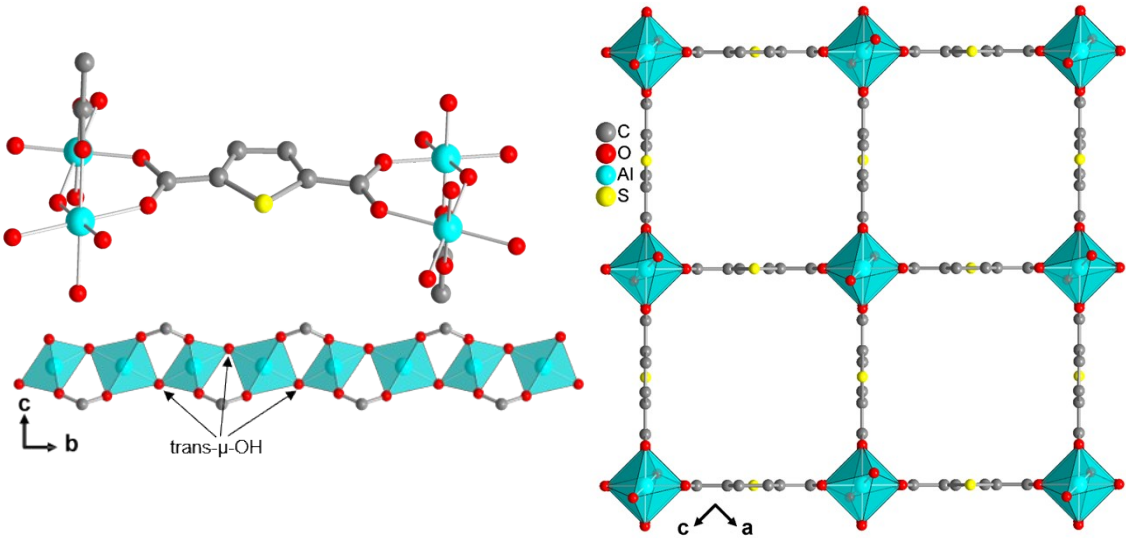

Fig. S4 Structural elements in MIL-53-TDC with extended asymmetric unit, the fourfold straight chain of trans vertex-bridged {AlO_6}-polyhedra as the inorganic building unit, and the 3D framework structure of square-shaped one-dimensional channels. Graphics produced from a cif-file provided by Serre and co-workers.

S3. Syntheses details

The synthesis of MIL-160, CAU-23 and the mixed 2,5-thiophenedicarboxylate-/2,5-furandicarboxylate (TF) MOF materials followed a uniform protocol adapted from Lenzen *et al.* albeit with lower amounts of the starting materials used and a different washing step. The molar ratio of $AlCl_3 \cdot 6H_2O$ and $NaAlO_2$ of 3:1 corresponds to the conditions by Lenzen *et al.*[3]

Table S1 Used and obtained linker ratios and yields of mixed MOF-syntheses.

Compound [a]	mol. ratio synthesis T : F	mol. ratio ^{1}H-NMR T : F [b]	n_{Al} ($AlCl_3$/$NaAlO_2$) [mmol] [c]	n_{H2FDC} [mmol]	n_{H2TDC} [mmol]	n_{NaOH} [mmol]	V_{H2O} [mL] [d]	Yield [g]	Yield [%]
CAU-23 (TF 99:01)	0.9 : 0.1	0.99 : 0.01	1.17/0.39	0.16	1.42	3.14	10	0.18	54
TF 95:05	0.8 : 0.2	0.95 : 0.05	4.69/1.57	1.26	5.04	12.63	25	0.98	74
TF 82:18	0.7 : 0.3	0.82 : 0.18	1.17/0.39	0.49	1.10	3.20	10	0.21	63
TF 72:28	0.6 : 0.4	0.72 : 0.28	1.17/0.39	0.63	0.95	3.18	10	0.21	64
TF 53:47	0.5 : 0.5	0.53 : 0.47	1.17/0.39	0.77	0.80	3.13	20	0.23	72
TF 38:62	0.4 : 0.6	0.38 : 0.62	1.17/0.39	0.94	0.63	3.18	10	0.22	70
TF 30:70	0.3 : 0.7	0.30 : 0.70	1.20/0.4	1.12	0.48	3.21	10	0.21	64
TF 18:82	0.2 : 0.8	0.18 : 0.82	4.69/1.56	5.01	1.26	12.59	25	0.94	74
TF 07:93	0.1 : 0.9	0.07 : 0.93	1.17/0.39	1.41	0.16	3.17	10	0.11	37
MIL-160	0 : 1	0.00 : 1.00	4.69/1.55	6.25	–	12.57	25	1.00	81

[a] The materials prepared from linker mixtures are denoted as TF xx:yy (T = TDC, F = FDC; xx = fraction of TDC, yy = fraction of FDC). [b] The values for the MOF-incorporated fractions of TDC and FDC were confirmed post-synthetically through solution ^{1}H NMR-spectroscopy with the MOFs dissolved (digested) in 5 % NaOD in D_2O (see Section S10). [c] Different aqueous storage solutions of $AlCl_3$ with c = 1.0 mol/L and of $NaAlO_2$ with c = 0.5 mol/L were used. [d] Volume of de-ionized H_2O used to dissolve the linker molecules.

Table S2 CHNS-Analysis results of mixed synthesis of TF with different ratios of TDC and FDC and corresponding molecular formulas determined by ^{1}H-NMR- analysis.

Sample	% C (calc.)	% H (calc.)	% S (calc.)	Molecular formula (^{1}H-NMR; CHNS-Analysis)
CAU-23(TF 99:01)	32.62 (32.82)	1.65 (1.66)	14.74 (14.46)	$[Al(OH)(TDC)_{0.99}(FDC)_{0.01}]\cdot 0.31\ H_2O$
TF 95:05	31.82 (32.47)	1.78 (1.79)	13.65 (13.73)	$[Al(OH)(TDC)_{0.95}(FDC)_{0.05}]\cdot 0.48\ H_2O$
TF 82:18	31.78 (30.98)	2.31 (2.33)	11.23 (11.30)	$[Al(OH)(TDC)_{0.82}(FDC)_{0.18}]\cdot 1.19\ H_2O$
TF 72:28	32.38 (31.86)	2.14 (2.16)	10.62 (10.21)	$[Al(OH)(TDC)_{0.72}(FDC)_{0.28}]\cdot 0.92\ H_2O$
TF 53:47	27.92(28.16)	3.31 (3.34)	6.69 (6.70)	$[Al(OH)(TDC)_{0.53}(FDC)_{0.47}]\cdot 2.73\ H_2O$
TF 38:62	33.19 (30.01)	2.91 (2.93)	5.54 (5.11)	$[Al(OH)(TDC)_{0.38}(FDC)_{0.62}]\cdot 1.99\ H_2O$
TF 30:70	33.38 (33.08)	2.14 (2.16)	4.02 (4.42)	$[Al(OH)(TDC)_{0.30}(FDC)_{0.70}]\cdot 0.83\ H_2O$
TF 18:82	31.85 (30.91)	2.82 (2.84)	2.69 (2.48)	$[Al(OH)(TDC)_{0.18}(FDC)_{0.82}]\cdot 1.79\ H_2O$
TF 07:93	35.75 (29.74)	3.21 (3.24)	1.07 (0.98)	$[Al(OH)(TDC)_{0.07}(FDC)_{0.93}]\cdot 2.39\ H_2O$
MIL-160	33.76 (34.54)	2.00 (2.02)	0.00 (0.00)	$[Al(OH)(FDC)]\cdot 0.59\ H_2O$

MIL-53-TDC

Table S3 Synthesis details of MIL-53-TDC.

Compound	$n_{Al2(SO4)3}$ [mmol]	n_{H2TDC} [mmol]	$m_{Al2(SO4)3}$ [g]	m_{H2TDC} [g]	V_{DMF} [mL]	V_{H2O} [mL]	Yield [g]	Yield [%]
MIL-53-TDC	1.79	1.57	1.19	0.27	3.14	10	0.30	90

S4. PXRD-measurements

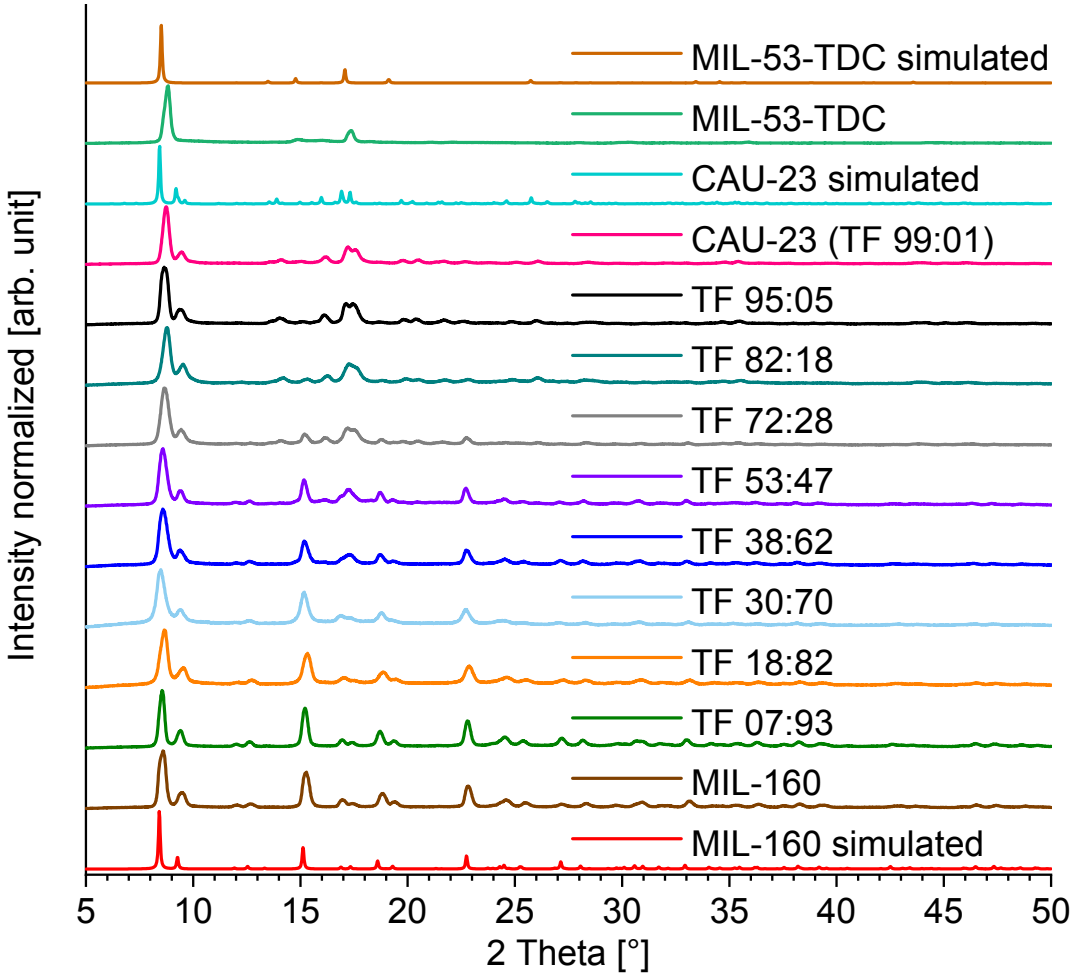

Fig. S5 PXRD patterns of mixed TF-MOF materials with varying ratios of TDC and FDC, MIL-160 and CAU-23 and simulated diffractograms of CAU-23 using a cif-file to CSD-Refcode ZOVHUQ[3] and MIL-160 from cif-file to CSD-Refcode PIBZOS.[1]

S5. IR spectroscopy

Infrared (IR) spectra of all samples are shown together with spectra of H_2TDC and H_2FDC in Fig. S6. An increasing fraction of TDC leads to the appearance of characteristic bands for TDC, e.g. ring vibrations at 1531 cm^{-1} ($\tilde{\nu}_{(C=C)}$) and 690 cm^{-1} ($\tilde{\nu}_{(C-S)}$).[1] An additional band around 1700 cm^{-1}, indicating the presence of carboxylic acid groups of free, uncoordinated linker molecules could not be observed. The asymmetric and symmetric stretch vibrations of carboxylate groups are visible around $\tilde{\nu}_{as(CO_2^-)}$ = 1640 and $\tilde{\nu}_{s(CO_2^-)}$ = 1420 cm^{-1}. Bands around 1580 cm^{-1} can be assigned to ring vibrations of TDC and FDC.[1]

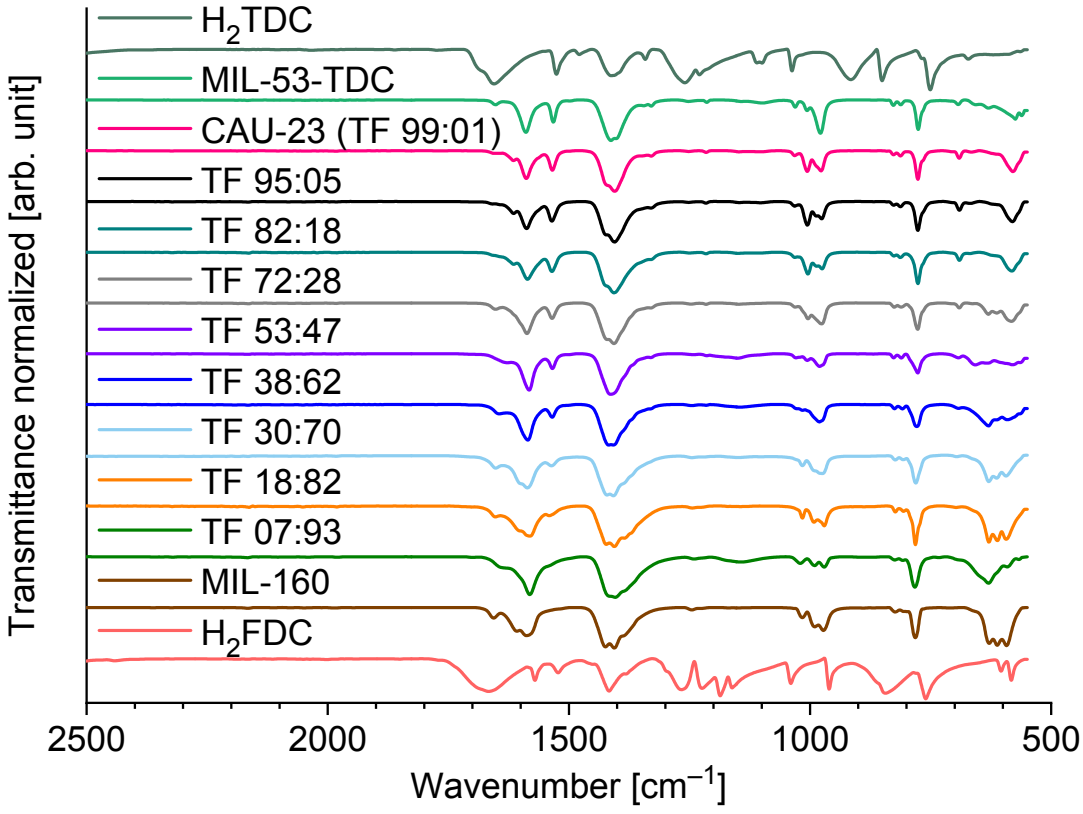

Fig. S6 IR spectra (ATR mode) of mixed MOFs in the range from 2500 to 550 cm^{-1}.

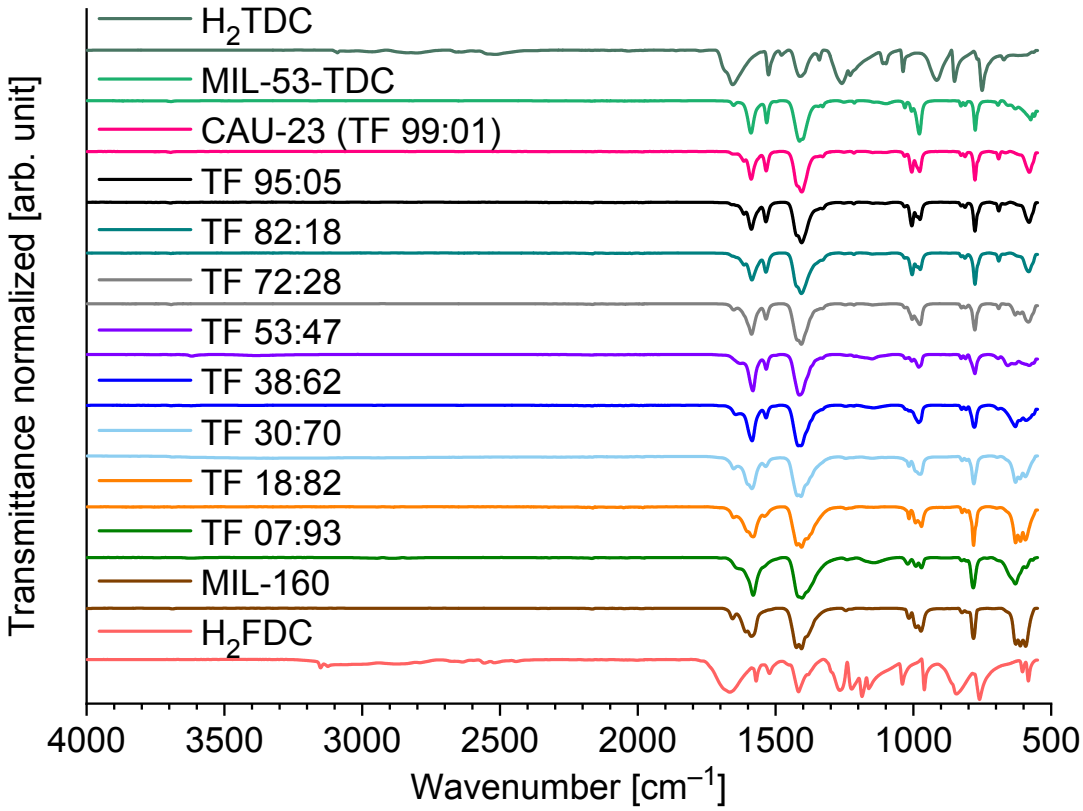

Fig. S7 Full IR spectra (ATR mode) of mixed TF materials with varying ratios of TDC and FDC in the range from 4000 to 550 cm^{-1}.

S6. Nitrogen sorption experiments (T = 77 K)

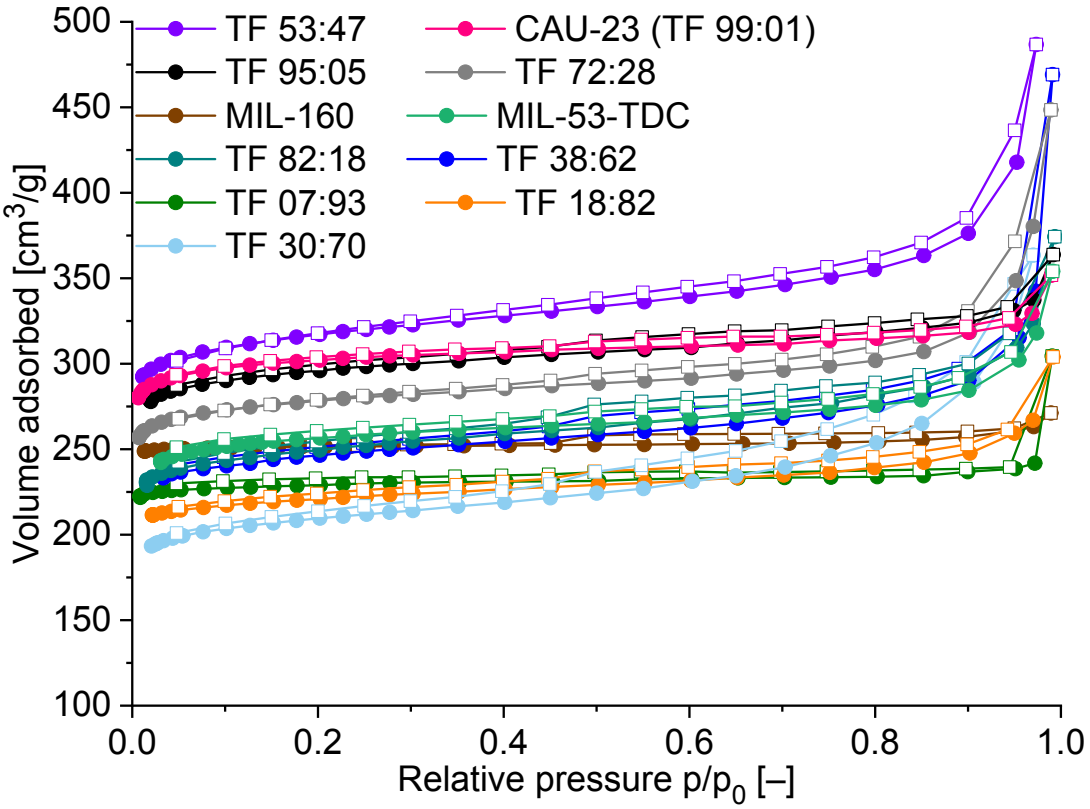

Fig. S8 N_2 sorption isotherms of mixed TF materials with different ratios of TDC (2,5-thiophenedicarboxylate) and FDC (2,5-furandicarboxylate) and all single-linker MOFs at 77 K. Filled symbols: adsorption; empty symbols: desorption.

S7. Water vapor sorption experiments (T = 293 K)

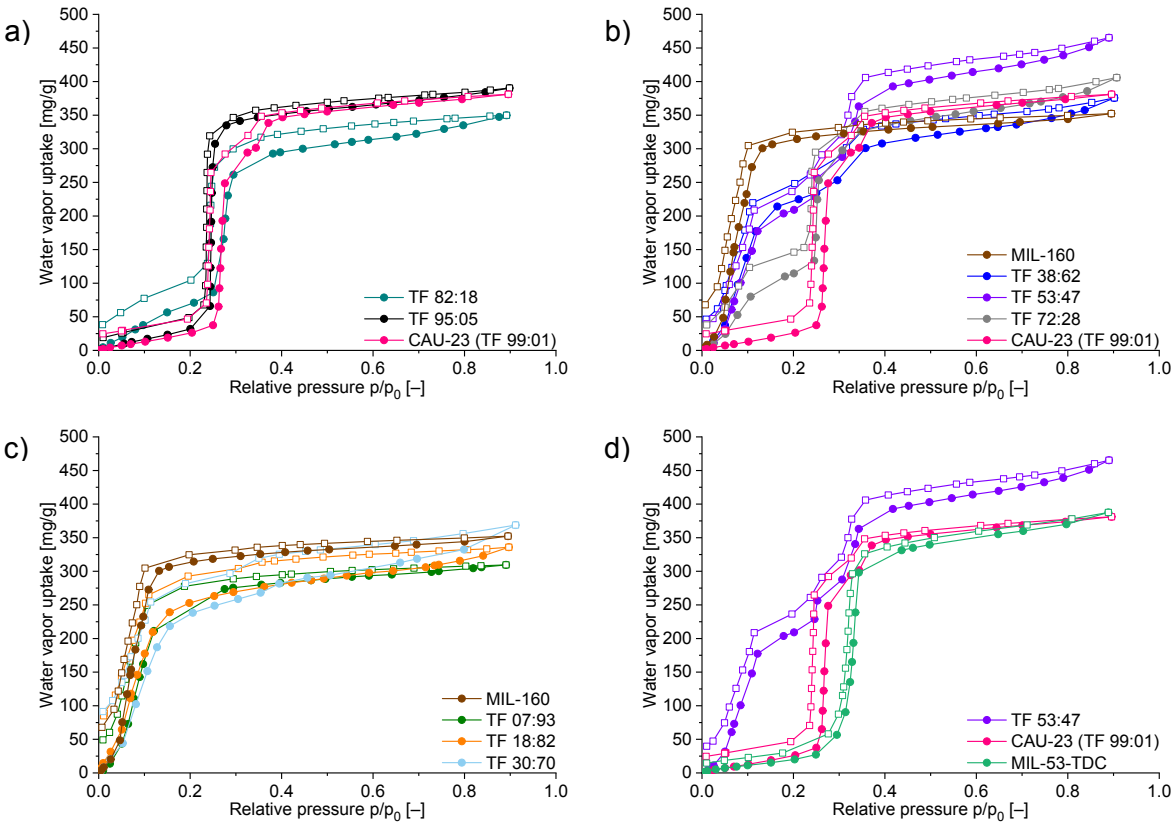

Fig. S9 Water vapor adsorption isotherms at 293 K for mixed TF-MOFs and single-linker MOFs (MIL-160 and MIL-53-TDC). a) Excess of TDC. b) Nearly equal amounts of both linkers. c) Excess of FDC. Filled symbols: adsorption; empty symbols: desorption.

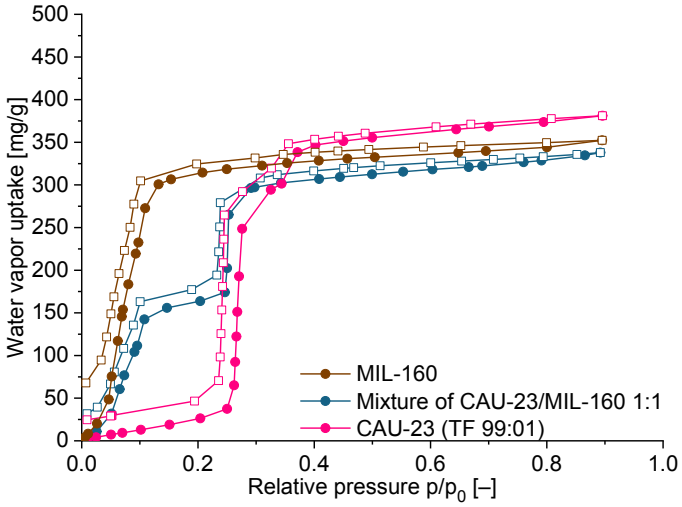

Fig. S10 Water vapor sorption isotherms at 293 K for CAU-23, MIL-160 and a 1:1 *ex-situ* mixture of both single-linker MOFs. Filled symbols: adsorption; empty symbols: desorption.

Capacities of all materials are listed in Table S4 and vary in the range of 238 – 393 mg/g (after uptake step) and 310 – 465 mg/g (total capacity). The published experimental total water capacity for MIL-160 is 370 mg/g at 303 K and was reproduced with an uptake value of 360 mg/g at 293 K in a sufficient way.[4] Whereas the high water uptake capacity values for CAU-23 (375 mg/g; 298 K; 0.33 p/p_0) reported by Lenzen *et al.* could not be reproduced, the best-achieved value was 271 mg/g (0.33 p/p_0) after uptake step and a saturation capacity of 319 mg/g.[3]

Table S4 Results of water sorption measurements of mixed TF

Compound TF x:y	Water vapor uptake [mg/g] at 293 K	
	After uptake steps	Total uptake
CAU-23 Lit.[3]	375 (0.33 p/p_0)[b]	–
CAU-23 (TF 99:01)	347 (0.40 p/p_0)	381 (0.90 p/p_0)
TF 95:05	341 (0.31 p/p_0)	390 (0.90 p/p_0)
TF 82:18	295 (0.40 p/p_0)	350 (0.89 p/p_0)
TF 72:28	335 (0.41 p/p_0)	406 (0.91 p/p_0)
TF 53:47	393 (0.42 p/p_0)	465 (0.89 p/p_0)
TF 38:62	308 (0.39 p/p_0)	376 (0.90 p/p_0)
TF 30:70	238 (0.21 p/p_0)	369 (0.91 p/p_0)
TF 18:82	253 (0.20 p/p_0)	336 (0.90 p/p_0)
TF 07:93	274 (0.28 p/p_0)	310 (0.90 p/p_0)
MIL-160	314 (0.20 p/p_0)	352 (0.90 p/p_0)
MIL-160 Lit.[4]		370[a]
MIL-53-TDC	331 (0.44 p/p_0)	387 (0.89 p/p_0)
MIL-53-TDC Lit.[5]		469[b] (0.9 p/p_0)

[a] Saturation capacity at 303 K reported by Cadiau *et al.*[4] [b] Capacity at 298 K[3,5]

An adsorbent material should fulfill the following requirements in order to be suitable for cycling water sorption in thermally driven adsorption heat pumps (AHPs):

(i) The sorption isotherm should have an S-shape (IUPAC classification Type V)[6] with a steep rise in the relative pressure range of $p/p_0 \approx 0.1–0.3$ for an effective profitable uptake in the adsorbent material.[7] The low uptake at low p/p_0 of the Type V isotherm can be attributed to relatively weak adsorbent–adsorbate interactions and illustrated the (low) hydrophilicity of the MOF. At higher p/p_0, water clustering is followed by pore filling. For instance, Type V isotherms are generally observed for water adsorption on hydrophobic microporous and mesoporous adsorbents. The pressure range can vary depending on the desired working conditions described above. The S-shape is advantageous because it enables a large lift of adsorption within a narrow relative pressure range.[8]

The adsorption of water vapor in MOFs occurs by three main mechanisms. 1. Adsorption of water molecules at low relative pressure (relative humidity) on open metal sites (chemisorption). 2. Cluster/layer formation in the pore system (reversible). 3. Continuous pore

filling (reversible) or capillary condensation (irreversible) depending on the pore size of the adsorbent. Below the critical diameter of water (D_c), reversible continuous pore filling takes place. D_c for water is about 20 Å at room temperature.[9]

In general, hydrophilic MOFs with a pore diameter <20 Å (microporous) show S-shaped water vapor sorption isotherms unless open metal sites lead to an additional uptake step at low relative pressure.[10]

For Al-MOFs with AlO_6-octahedral chains no open metal sites are known, therefore the first water molecules form hydrogen bonds to the bridging μ-OH-sites of the AlO_6-octahedra. These adsorbed water molecules then act as nucleation sites for additional molecules and lead to the formation of larger water clusters. As loading increases continuously, separate water clusters connect under formation of hydrogen bonds, leading to a complete pore filling.[2,3,11]

The relative pressure, where the steep water uptake takes place, depends mainly on the pore size and the hydrophilicity of the used linker molecules. Smaller pore sizes and more hydrophilic linkers lead to a shift of the water uptake to lower relative pressures.[10,12]

In a mixed-linker MOF with statistical distribution of the linker molecules, the hydrophilicity should change according to the incorporation of the differently hydrophilic linkers. Therefore, the uptake step should shift in-between the steps of the neat MOFs.

S8. Scanning electron microscopy (SEM)

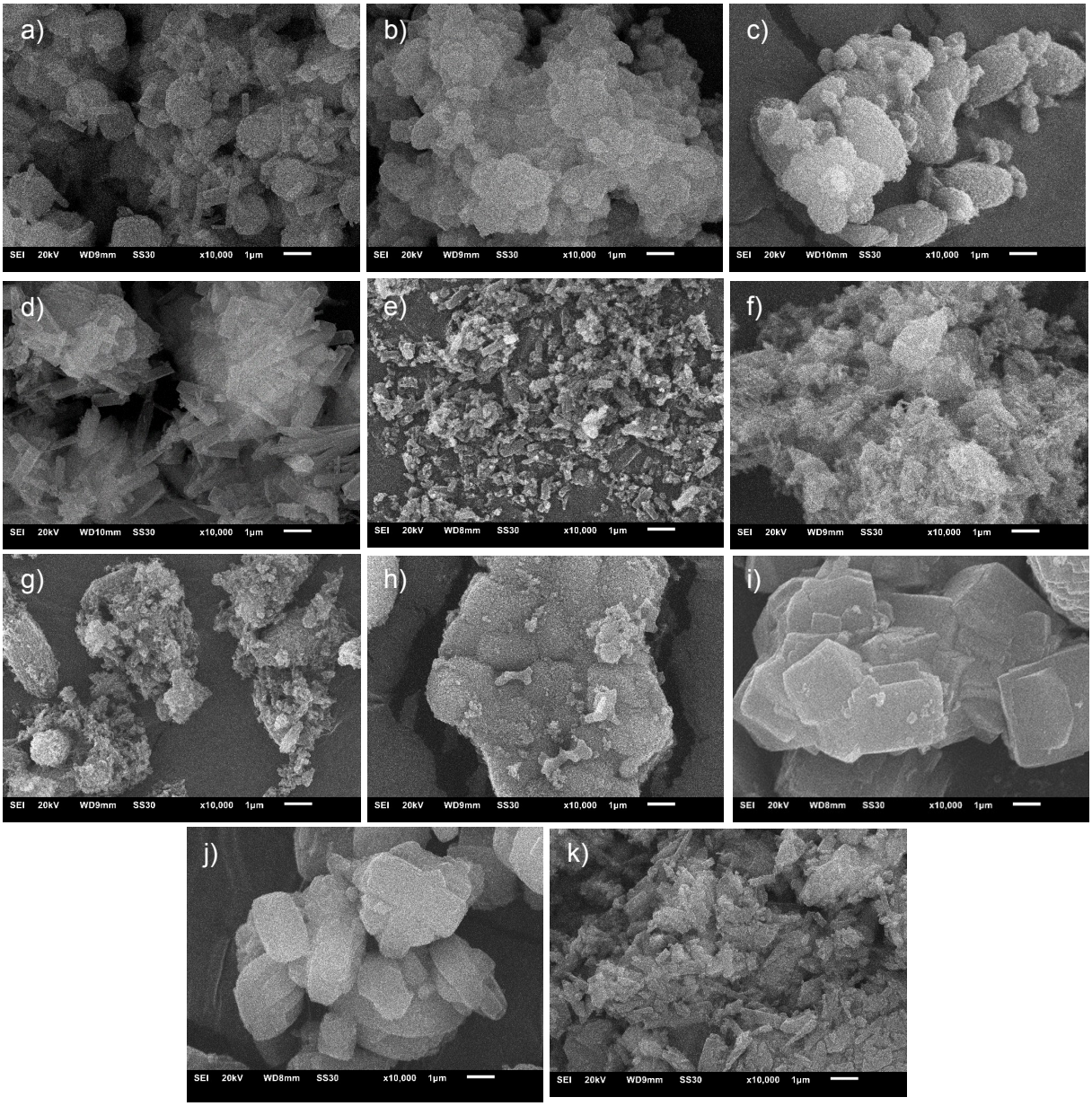

Fig. S11 SEM images of synthesized mixed materials with different ratios of TDC and FDC. a) CAU-23(TF 99:01), b) TF 95:05, c) TF 82:18, d) TF 72:28, e) TF 53:47, f) TF 38:62, g) TF 30:70, h) TF 18:82, i) TF 07:93, j) MIL-160, k) MIL-53-TDC. Magnification in all images is 10 000; the scale bar is 1 μm.

S9. Thermogravimetric analysis (TGA)

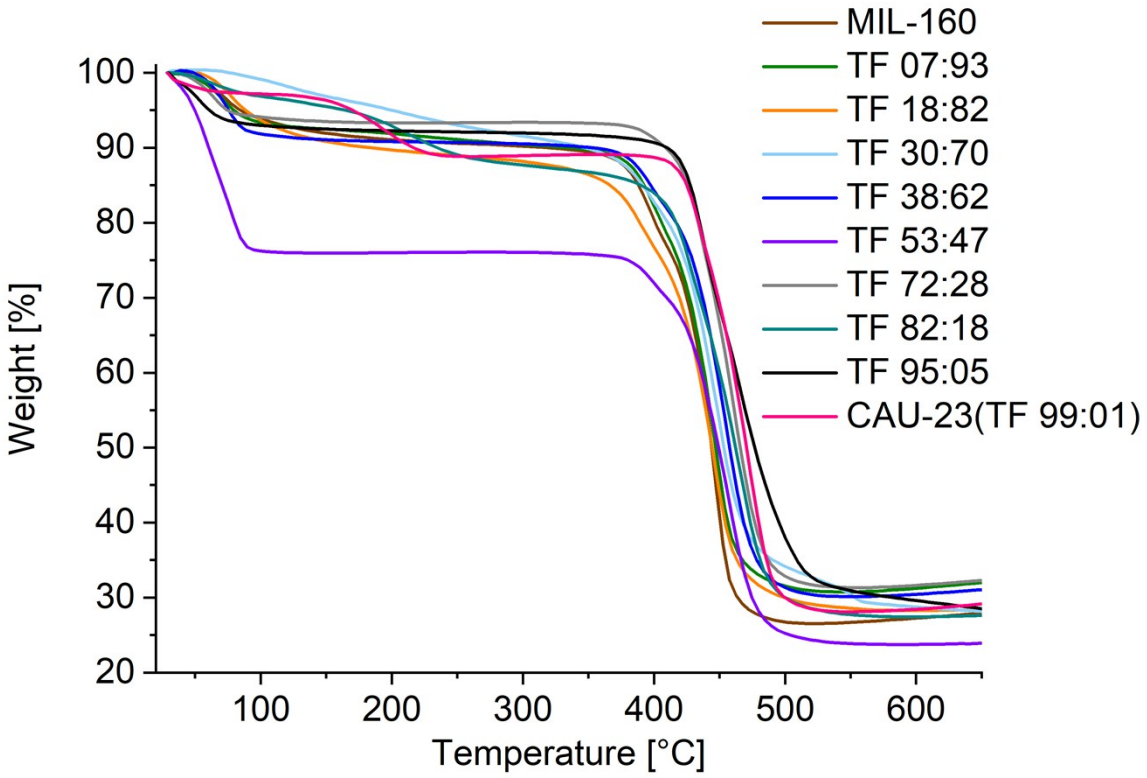

Fig. S12 TGA results of synthesized mixed materials with different ratios of TDC and FDC under synthetic air atmosphere.

Table S5 Results of TGA-measurements of single-linker MOFs and mixed TF materials.

Compound	First weight loss y [%]	Second weight loss [%] (calc.) [a]	Residue mass [%] (calc.) [a]
CAU-23 (TF 99:01)	11.0 [b]	60.9 (64.5)	28.1 (24.5)
TF 95:05	7.9	63.6 (66.8)	28.5 (25.3)
TF 82:18	12.9 [b]	59.7 (63.4)	27.4 (23.7)
TF 72:28	6.7	62.0 (68.0)	31.3 (25.3)
TF 53:47	24.0	52.3 (55.7)	23.7 (20.3)
TF 38:62	9.3	60.6 (66.7)	30.1 (24.0)
TF 30:70	8.6	63.7 (67.4)	27.7 (24.1)
TF 18:82	11.5	59.9 (65.4)	28.2 (23.1)
TF 07:93	8.7	60.5 (67.7)	30.8 (23.6)
MIL-160	9.5	64.0 (67.2)	26.5 (23.3)

[a] For the evaluation the formula $[Al(OH)(TDC)]_{T/100}[Al(OH)(FDC)]_{F/100} \cdot y/100H_2O$ was used. The molar fractions of TDC and FDC had been determined postsynthetically by digestion NMR in 5 % NaOD in D_2O (see Section S3 and S10). The water content of the materials varied with the air moisture, therefore we assigned the first weight loss to the desorption of water and adjusted the experimental formula accordingly.

The calculated values differ within a 3-7 wt% from the observed values, such that the mass loss for the ligand is lower, the residue mass of Al_2O_2S for CAU-23,[3] and Al_2O_3 for MIL-160 is concomitantly higher than calculated. We can explain this deviation either by the formation of Al-salt residues (including $Al(OH)_3$ hydrolysis products) or to the formation of missing-linker defects during the synthesis of the materials. Missing-linker defects can influence the surface area and pore volume in either direction.[13,14]

[b] Two weight losses under 300 °C

S10. ^{1}H-NMR-spectra of dissolved compounds

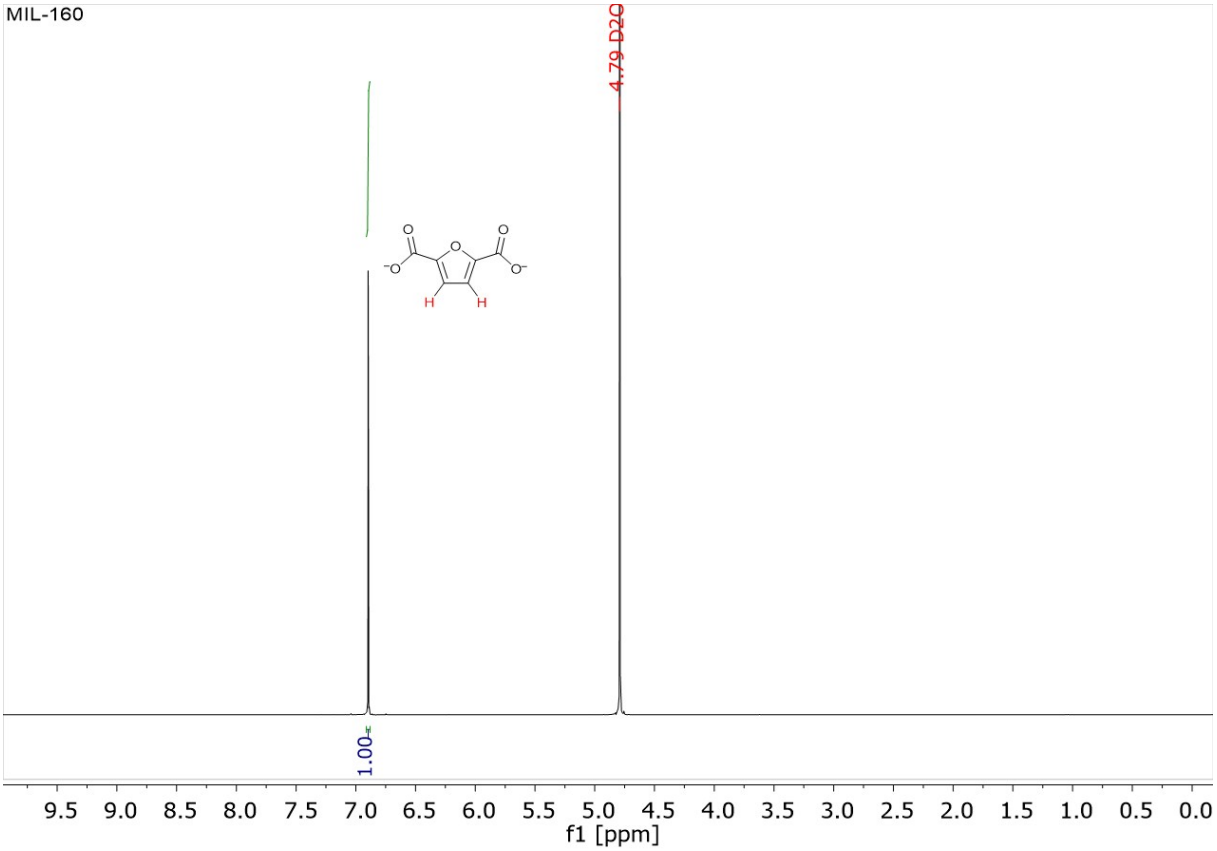

Fig. S13 ^{1}H-NMR spectrum of MIL-160 after dissolution in 5 % NaOD in D_2O.

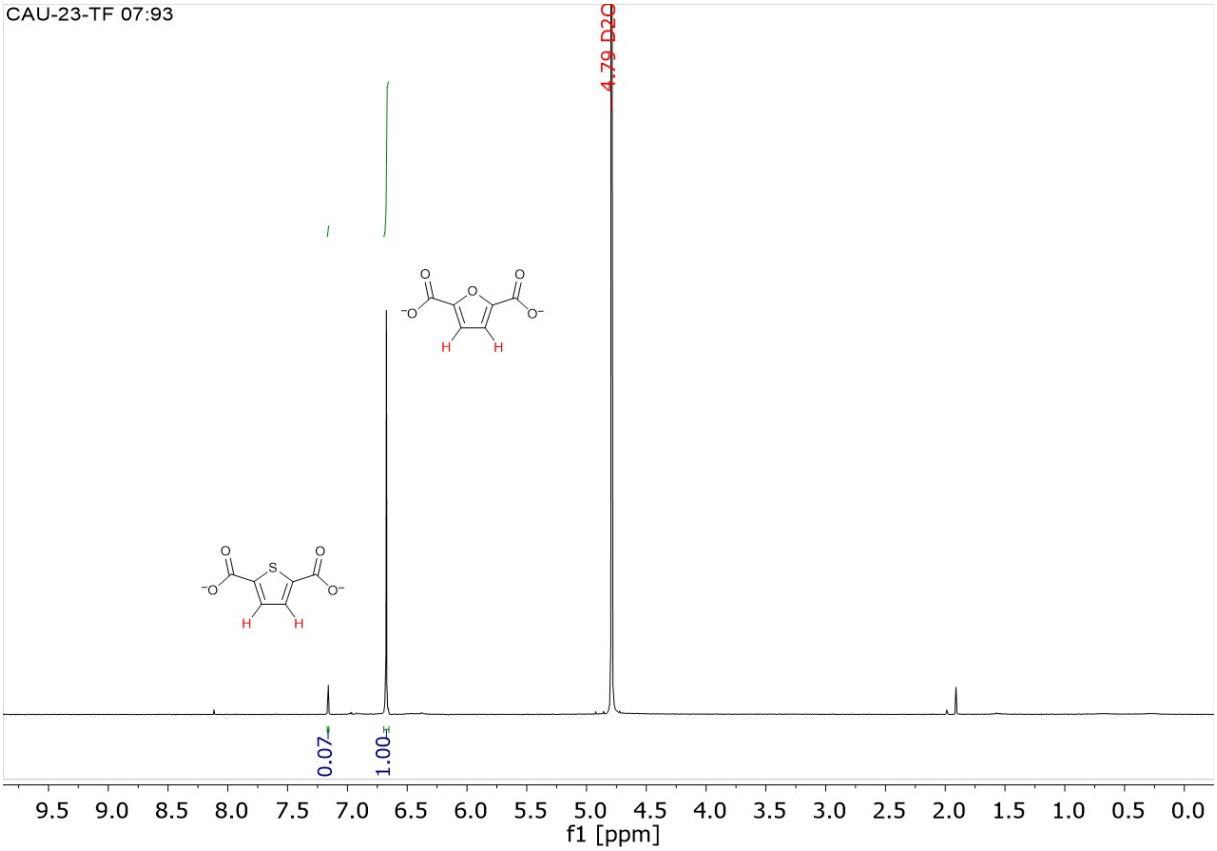

Fig. S14 ^{1}H-NMR spectrum of TF 07:93 after dissolution in 5 % NaOD in D_2O.

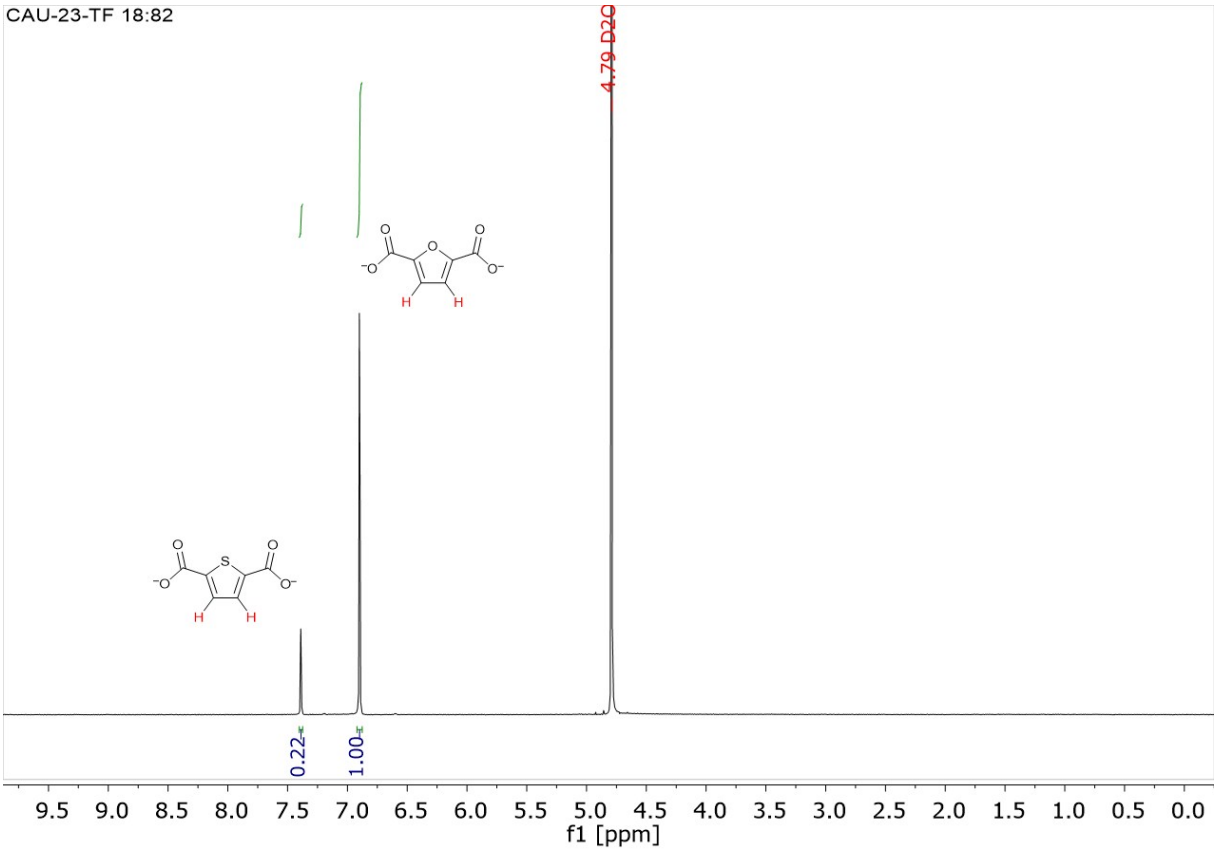

Fig. S15 ^{1}H-NMR spectrum of TF 07:93 after dissolution in 5 % NaOD in D_2O.

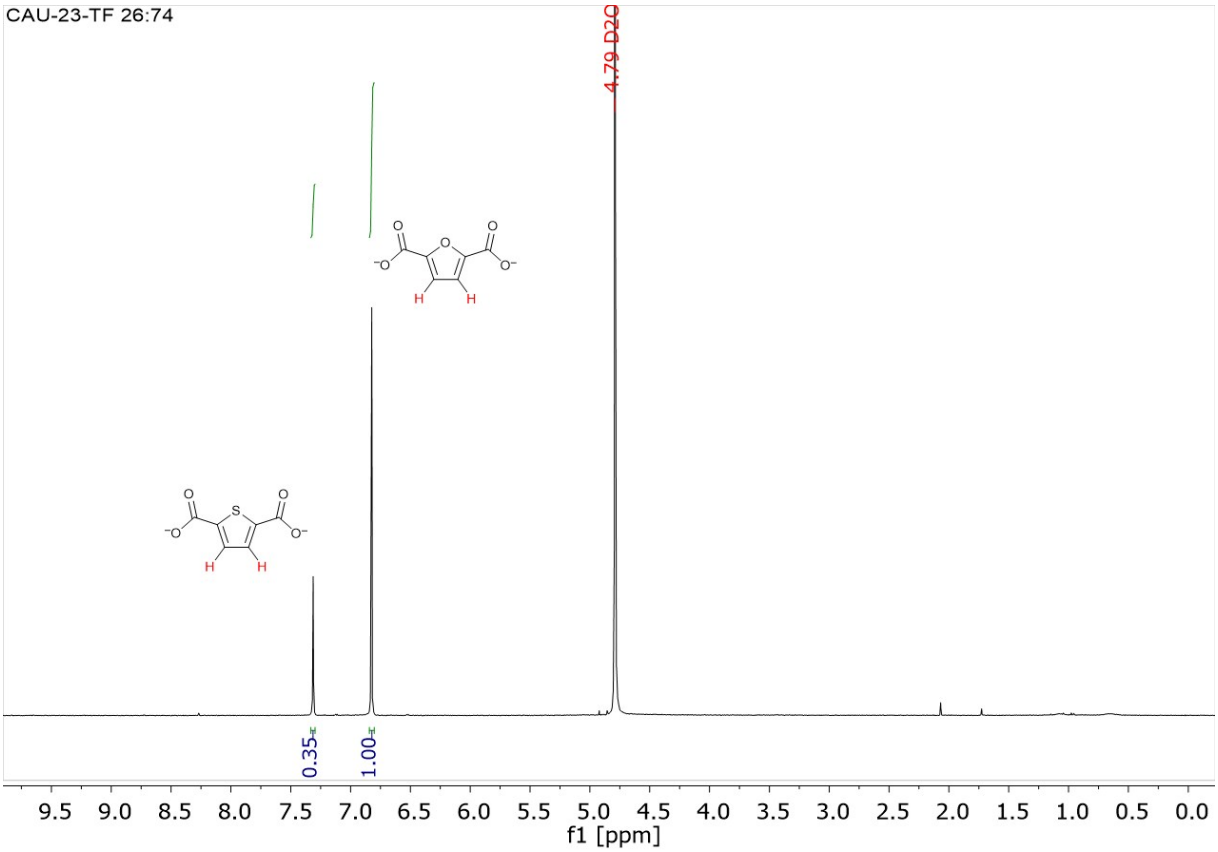

Fig. S16 ^{1}H-NMR spectrum of TF 18:82 after dissolution in 5 % NaOD in D_2O.

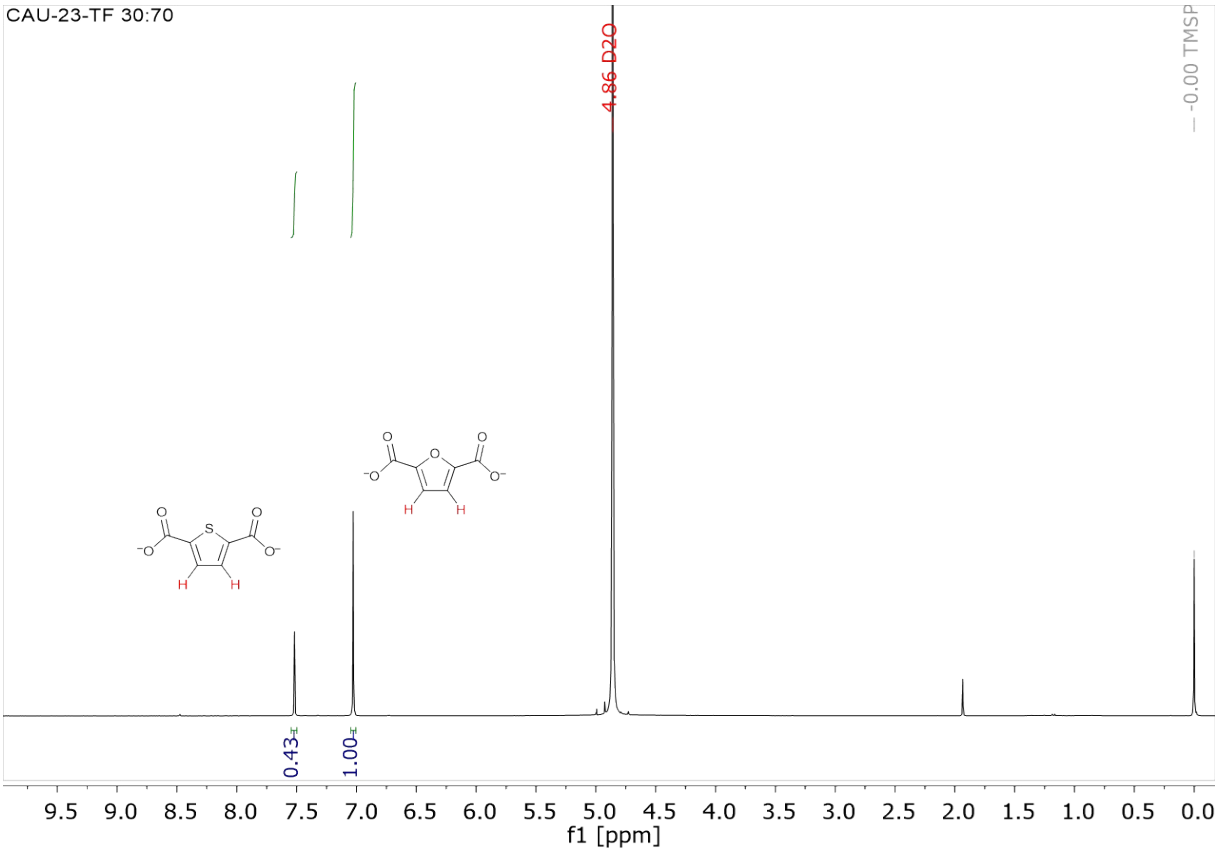

Fig. S17 ^{1}H-NMR spectrum of TF 30:70 after dissolution in 5 % NaOD in D_2O.

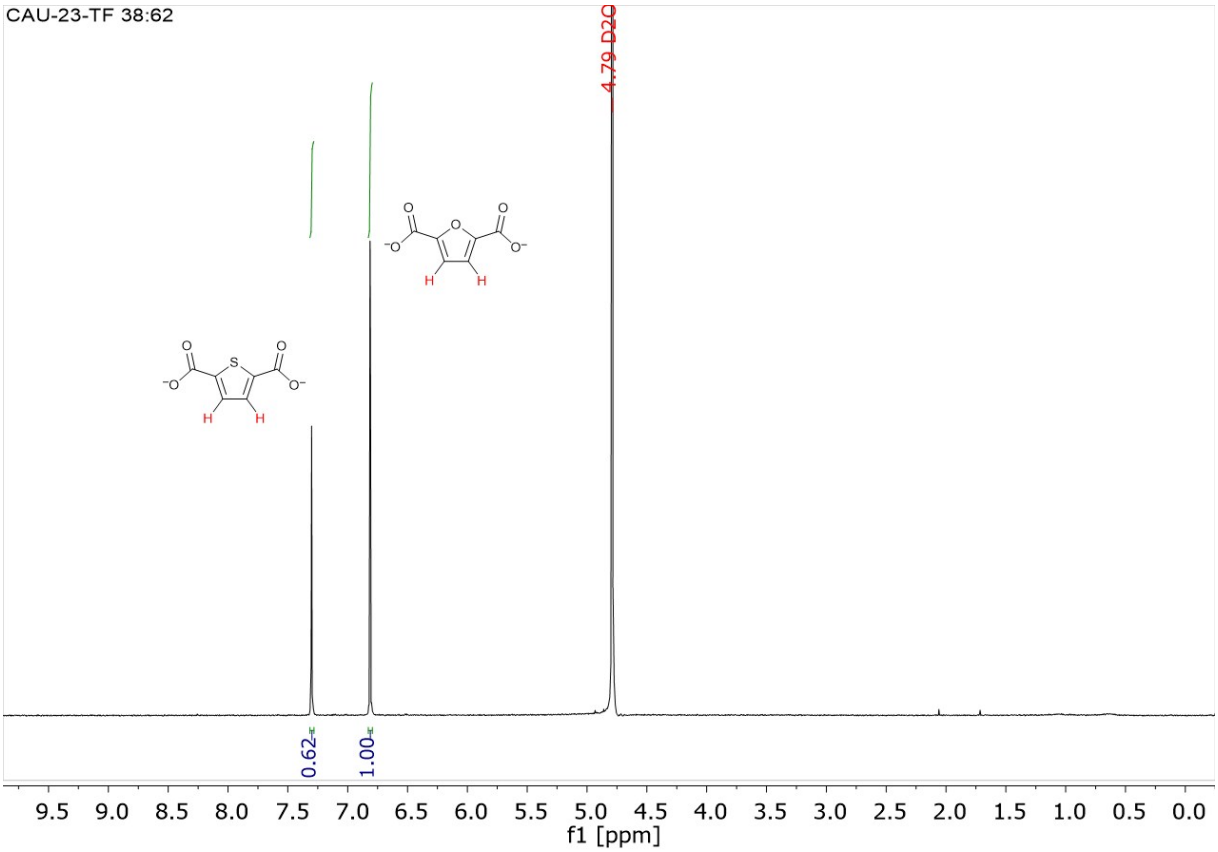

Fig. S18 ^{1}H-NMR spectrum of TF 38:62 after dissolution in 5 % NaOD in D_2O.

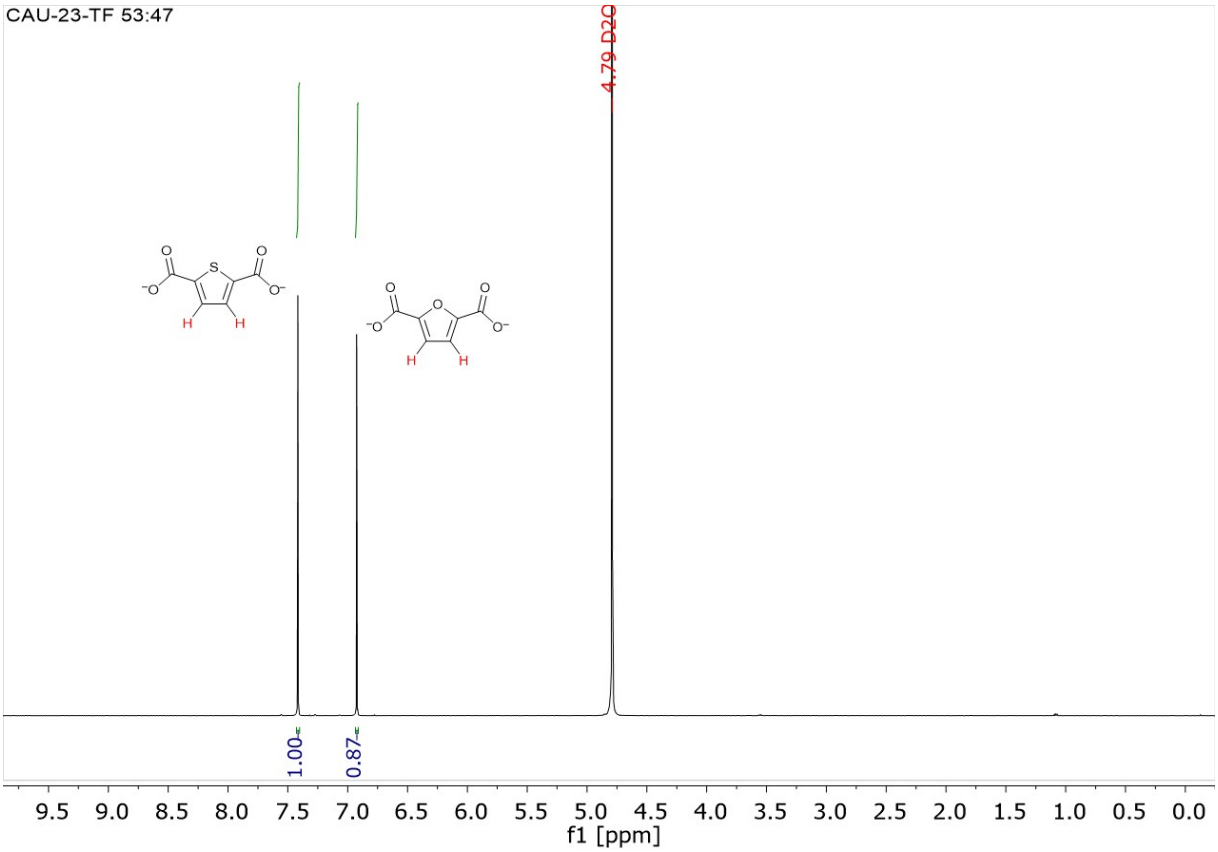

Fig. S19 ^{1}H-NMR spectrum of TF 53:47 after dissolution in 5 % NaOD in D_2O.

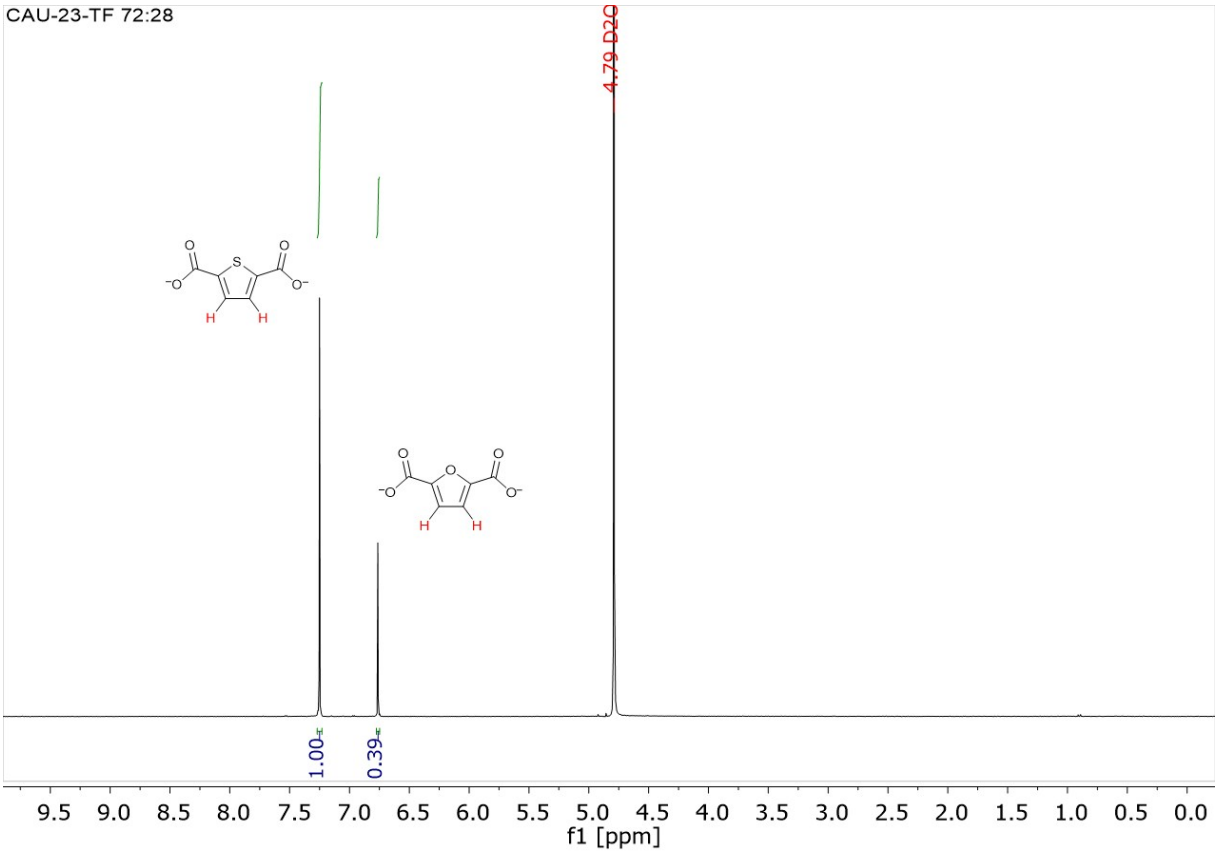

Fig. S20 ^{1}H-NMR spectrum of TF 72:28 after dissolution in 5 % NaOD in D_2O.

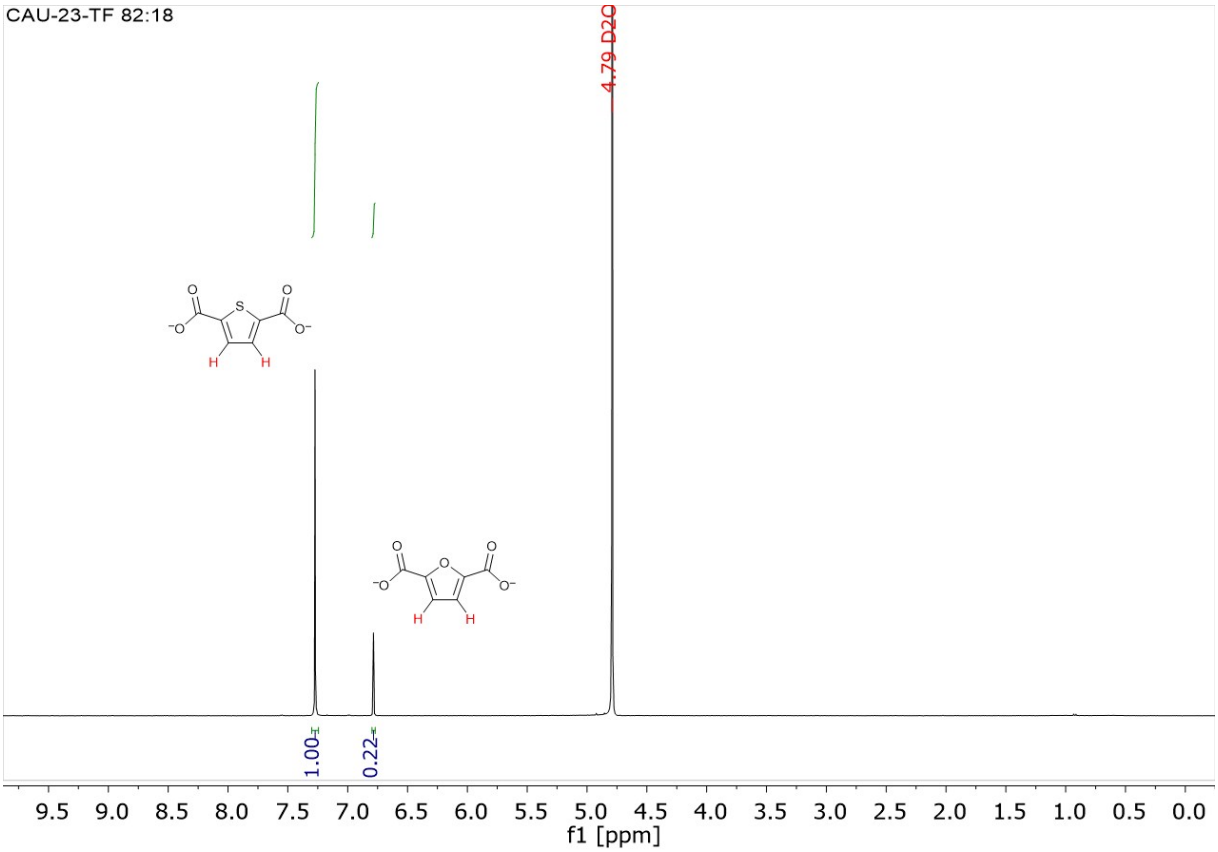

Fig. S21 ^{1}H-NMR spectrum of TF 82:18 after dissolution in 5 % NaOD in D_2O.

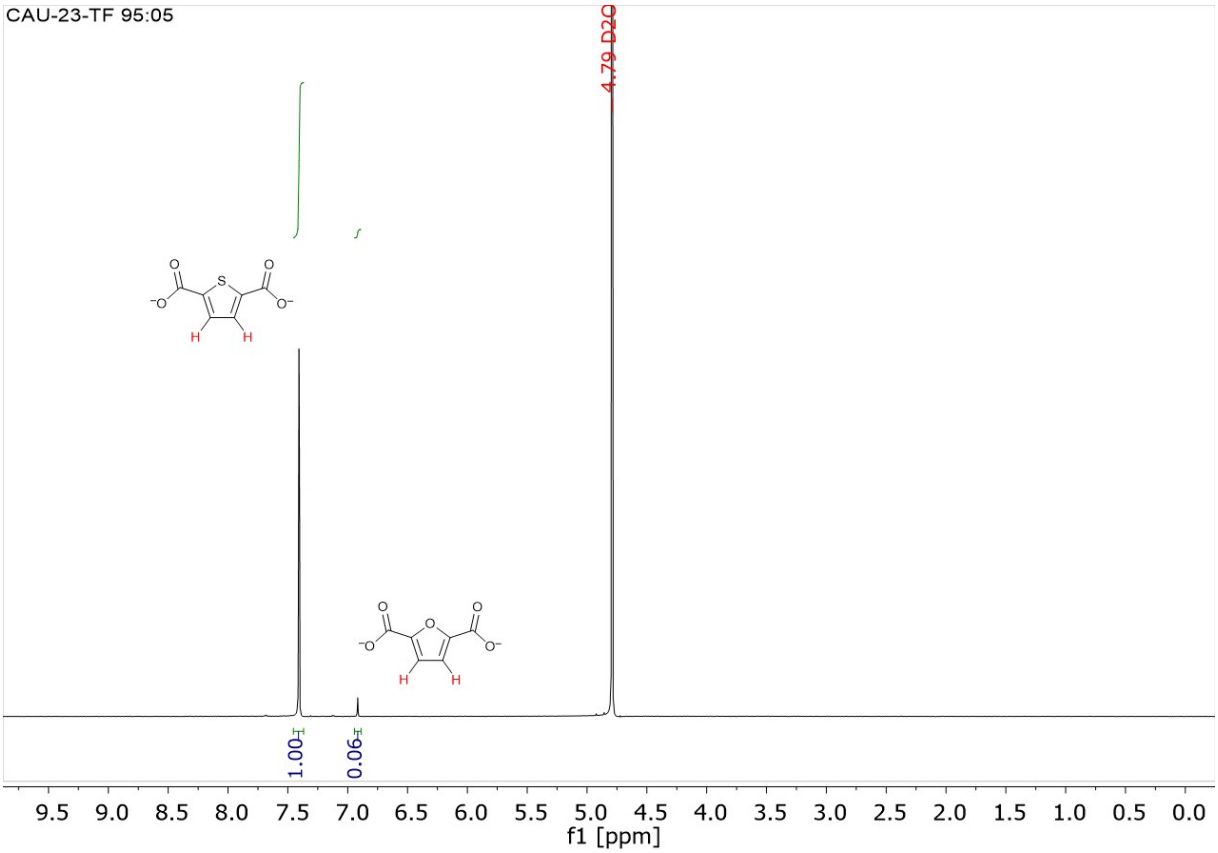

Fig. S22 ^{1}H-NMR spectrum of TF 95:05 after dissolution in 5 % NaOD in D_2O.

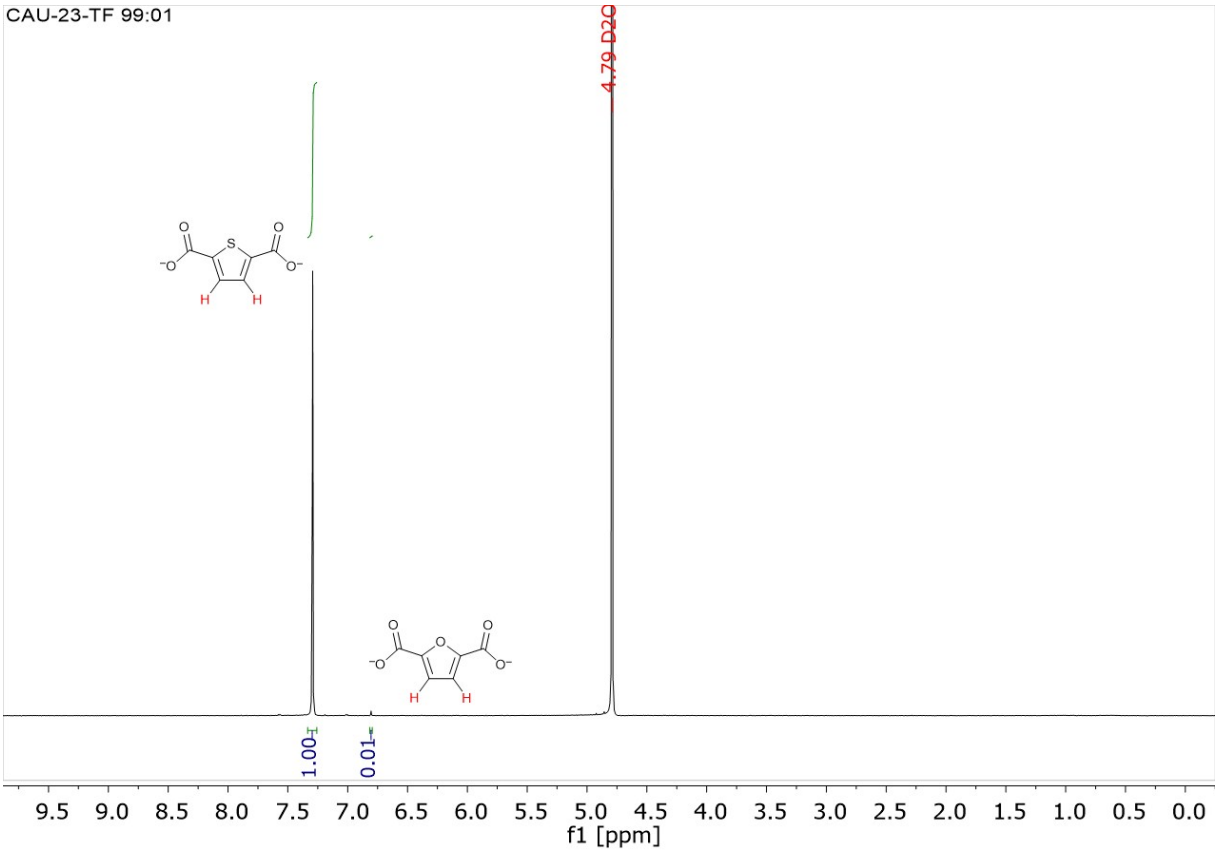

Fig. S23 ^{1}H-NMR spectrum of CAU-23 (TF 99:01) after dissolution in 5 % NaOD in D_2O.

References

1 M. Wahiduzzaman, D. Lenzen, G. Maurin, N. Stock and M. T. Wharmby, *Eur. J. Inorg. Chem.*, 2018, 3626–3632.

2 D. Fröhlich, E. Pantatosaki, P. D. Kolokathis, K. Markey, H. Reinsch, M. Baumgartner, M. A. van der Veen, D. E. de Vos, N. Stock, G. K. Papadopoulos, S. K. Henninger and C. Janiak, *J. Mater. Chem. A*, 2016, **4**, 11859–11869.

3 D. Lenzen, J. Zhao, S.-J. Ernst, M. Wahiduzzaman, A. Ken Inge, D. Fröhlich, H. Xu, H.-J. Bart, C. Janiak, S. Henninger, G. Maurin, X. Zou and N. Stock, *Nat. Commun.*, 2019, **10**, 3025.

4 A. Cadiau, J. S. Lee, D. Damasceno Borges, P. Fabry, T. Devic, M. T. Wharmby, C. Martineau, D. Foucher, F. Taulelle, C.-H. Jun, Y. K. Hwang, N. Stock, M. F. de Lange, F. Kapteijn, J. Gascon, G. Maurin, J.-S. Chang and C. Serre, *Adv. Mater.,* 2015, **27**, 4775–4780

5 C. B. L. Tschense, N. Reimer, C.-W. Hsu, H. Reinsch, R. Siegel, W.-J. Chen, C.-H. Lin, A. Cadiau, C. Serre, J. Senker and N. Stock, *Z. Anorg. Allg. Chem.,* 2017, **643**, 1600–1608.

6 M. Thommes, K. Kaneko, A. V. Neimark, J. P. Olivier, F. Rodriguez-Reinoso, J. Rouquerol and K. S.W. Sing, *Pure Appl. Chem.*, 2015, **87**, 1051–1069.

7 Y. I. Aristov, *Applied Thermal Engineering*, 2013, **50**, 1610–1618.

8 S. K. Henninger, F. Jeremias, H. Kummer and C. Janiak, *Eur. J. Inorg. Chem.*, 2012, 2625–2634.

9 J. Canivet, A. Fateeva, Y. Guo, B. Coasne and D. Farrusseng, *Chem. Soc. Rev.,* 2014, **43**, 5594–5617.

10 O. M. Yaghi, M. J. Kalmutzki and C. S. Diercks, eds., Introduction to Reticular Chemistry. Metal-organic frameworks and covalent organic frameworks, Wiley, Weinheim, 2019.

11 H. Furukawa, F. Gándara, Y.-B. Zhang, J. Jiang, W. L. Queen, M. R. Hudson and O. M. Yaghi, *J. Am. Chem. Soc.;* 2014, **136**, 4369–4381.

12 M. F. de Lange, K. J. F. M. Verouden, T. J. H. Vlugt, J. Gascon and F. Kapteijn, *Chem. Rev.*, 2015, **115**, 12205–12250.

13 T. J. Matemb Ma Ntep, H. Reinsch, C. Schlüsener, A. Goldman, H. Breitzke, B. Moll, L. Schmolke, G. Buntkowsky and C. Janiak, *Inorg. Chem.*, 2019, **58**, 10965–10973.

14 M. J. Cliffe, W. Wan, X. Zou, P. A. Chater, A. K. Kleppe, M. G. Tucker, H. Wilhelm, N. P. Funnell, F.-X. Coudert and A. L. Goodwin, *Nat. Commun.*, 2014, **5**, 4176.